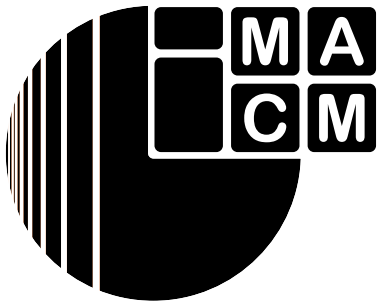


Bergische Universität Wuppertal

Fachbereich Mathematik und Naturwissenschaften

Institute of Mathematical Modelling, Analysis and Computational Mathematics (IMACM)

Preprint BUW-IMACM 19/30

Pavel S. Petrov, Matthias Ehrhardt, Andrey G. Tyshchenko and Petr N. Petrov

# Wide-angle mode parabolic equations for the problems of underwater acoustics and their numerical solution on unbounded domains

November 2019

http://www.math.uni-wuppertal.de

# Wide-angle mode parabolic equations for the problems of underwater acoustics and their numerical solution on unbounded domains

Pavel S. Petrov[a], Matthias Ehrhardt[b], Andrey G. Tyshchenko[c,a], Petr N. Petrov[d,e]

[a] *Il'ichev Pacific oceanological institute, 43 Baltiyskaya str., Vladivostok, 690041, Russia*
[b] *Bergische Universität Wuppertal, Gaußstrasse 20, D-42119 Wuppertal, Germany*
[c] *Far Eastern Federal University, 8 Sukhanova str., 690950, Vladivostok, Russia*
[d] *Moscow Institute of Physics and Technology, 9 Institutskiy Per., Dolgoprudny, Moscow oblast, 141701, Russia*
[e] *Ishlinskii Institute for Problems in Mechanics, 101-1 Vernadskogo Ave., Russian Academy of Sciences, Moscow, 119526, Russia*

**Abstract**

The modelling of sound propagation in the ocean by the solution of mode parabolic equations is concisely discussed. Mode parabolic equations can be obtained as the one-way approximation to horizontal refraction equations for modal amplitudes. Their wide-angle capabilities depend on the order of the Padé approximation of the involved pseudo-differential operators.

Various aspects of numerical solution methods for wide-angle mode parabolic equations are considered in detail, including artificial domain truncation and Cauchy initial data for the point source field approximation. The skills of the discussed numerical approaches are demonstrated in several important test cases, including the problems of sound propagation in a penetrable wedge and in a sea with an underwater canyon.

*Keywords:* underwater acoustics, horizontal refraction, wide-angle mode parabolic equation, transparent boundary conditions, starter, penetrable wedge, underwater canyon

*2010 MSC:* 65M06, 76Q05, 35S10

*Email addresses:* petrov@poi.dvo.ru (Pavel S. Petrov), ehrhardt@uni-wuppertal.de (Matthias Ehrhardt), ggoldenfeniks@gmail.com (Andrey G. Tyshchenko), petr.petrov@phystech.edu (Petr N. Petrov)

## 1. Introduction

The representation of an acoustic field in a 3D shallow-water waveguide in the form of a modal decomposition leads to 2D Helmholtz-type equations for the modal amplitudes [1, 2, 3] (see Eq. (2) below). They are often called *horizontal refraction equations* (HREs). Many techniques were developed for the solution of HREs since they appeared in the literature in 1970s for the first time, including ray theory [2], parabolic approximation [4] and a variety of analytical methods (see, e.g., [3]).

Parabolic approximations to HREs also known as *mode parabolic equations* (MPEs) were first introduced in ocean acoustics in 1993 by Collins [4] and later independently also derived by Trofimov [5]. Although in the pioneering studies mode coupling effects in the MPE propagation models were neglected, in later works Abawi et al [6] and Trofimov et al [7] also proposed systems of MPEs that take mode interaction into account. From [7] it is clear however that narrow-angle MPEs with mode interaction terms fail to accurately describe important horizontal refraction effects. In principle, narrow-angle MPEs can be solved numerically by exactly the same methods as Schrödinger equations and (paraxial) parabolic equations from optics and radiophysics (e.g., by finite differences, exponential time differencing, split-step Fourier and many other methods [1]). In some important cases MPEs also admit analytical solutions by group-theoretical technique [8, 9, 10].

Although usually mode coupling is considered more important for propagation models in underwater acoustics than their wide-angle capabilities in the horizontal plane, recent results [11] indicate that, on the contrary, the latter feature is crucial for handling many practical problems. To our knowledge, until now little attention was paid in the literature to the derivation, validation and numerical solution of *wide-angle mode parabolic equations* (WAMPEs). The aim of this work is two-fold. Firstly, we provide a comprehensive description of state-of-the-art numerical approaches that can be used for adiabatic WAMPE

solution. This description covers such issues as very-wide-angle numerical propagators, artificial domain truncation, and the design of the initial condition for the modelling of an omnidirectional point source. Secondly, we present a collection of numerical examples that demonstrate the performance of the numerical methods and the accuracy of 3D acoustical fields simulation. In this study we do not take mode interaction effects into account, and from our results one can conclude that in many cases they are of secondary importance as compared to the horizontal refraction effects. Our work will be also used as a basis for the development of WAMPE theory with mode interaction in future.

In our opinion, WAMPEs are a very useful alternative to omnivorous but somewhat computationally inefficient three-dimensional parabolic equations (3D PEs). Formally, a system of WAMPEs can be considered a result of model order reduction procedure [12] applied to a 3D PE, since the field in the vertical dimension for which one normally needs at least several hundreds of discretization points is represented by a combination of acoustical modes (usually no more than a dozen is necessary). Thus, the computations can be performed much faster even for a coupled system of mode parabolic equations for the modal amplitudes. The solution is simplified even further in the case of adiabatic (uncoupled) WAMPEs (and very often this does not really affect accuracy in any significant way).

WAMPEs can be solved both in polar [4] and in Cartesian [5] coordinate systems. We find it more practical to use the latter one, since on one hand this somewhat better fits practical problems (see, e.g., [13, 14], and, on the other hand, does not require any tessellation of the grid (increasing azimuthal sampling at long range from the source) which is often needed for the solution of wave propagation problems in polar coordinates.

An inherent feature of MPEs is that they are always solved on unbounded domains (by contrast to “normal”, or “vertical” parabolic equations in underwater acoustics which are solved in a stack of layers that have ocean surface as their upper boundary and, at least in theory, some lower boundary at the sea bottom as well). Thus, a proper artificial truncation of the computational

domain in $y$-direction is an inevitable step of a numerical solution of such equations. This truncation approach should of course change the model as little as possible. At artificial boundaries one has to set up perfectly matched layers (PMLs) or transparent/absorbing boundary conditions (TBCs/ABCs). Another important of the parabolic equations approach is the proper choice of the initial (Cauchy) data, also called a PE starter. In underwater acoustics starters are usually designed in such a way that the PE solution approximates the solution of the respective Helmholtz equation with a point source on the right-hand side. All these issues are discussed in the present work in the context of MPEs.

The paper is organized as follows. In Section 2 we introduce horizontal refraction equations (HREs) and use them as a basis for the derivation of pseudo-differential mode parabolic equations (PDMPEs) in Section 3. Next, in Section 4 we turn to the numerical solution discussing first high-order Padé mode parabolic equations in §4.1 and the split-step Padé (SSP) solution approach for the PDMPE in §4.2. Later we describe the finite difference discretization of the operator $L$ in §4.3. In Section 5 we discuss artificial truncation of the computational domain in the horizontal $y$-direction using PML (§5.1) or discrete TBCs (§5.2). Next, in Section 6, we describe different initial data ('starters') modelling a point source that can be used to initialize the solution of a WAMPE. Finally, in Section 7 we present some numerical examples to illustrate the accuracy of the WAMPE-based computational model in various propagation scenarios of shallow-water acoustics and to compare the three starters discussed in Section 6.

We provide the code used in the numerical examples in this work as supplementary material. High-order Padé MPEs solution scheme with fully-discrete TBCs was implemented in C++ [15], while the SSP method implementation with PMLs for the artificial domain truncation was accomplished in MATLAB [16]. The figures presented in §7 were obtained using a MATLAB version of the SSP solution algorithm, but the C++ code produces absolutely identical results.

## 2. The Horizontal Refraction Equation

The sound field $p(x, y, z)$ produced by a time-harmonic point source in a 3D shallow-water waveguide is described by the three-dimensional Helmholtz equation (where $z$ denotes the depth, and $x$, $y$ are the horizontal coordinates). Its solution can be expressed in the form of the modal decomposition [1, 3]

$$p(x, y, z) = \sum_{j=1}^{J} A_j(x, y)\, \varphi_j(z, x, y), \quad z > 0, \tag{1}$$

where $\varphi_j(z, x, y)$ are the modal functions [1] and $A_j(x, y)$ denote the modal amplitudes. Under the adiabatic assumption modal amplitudes satisfy the so-called (uncoupled) *horizontal refraction equation (HRE)* [1, 2, 10]:

$$\frac{\partial^2 A_j}{\partial x^2} + \frac{\partial^2 A_j}{\partial y^2} + k_j^2(x, y) A_j = -\varphi_j(z_s)\, \delta(x)\delta(y), \qquad j = 1, \dots J, \tag{2}$$

where $k_j = k_j(x, y)$ are the modal wavenumbers, and $z_s$ denotes the source depth. The modal functions $\varphi_j(z, x, y)$ and the respective horizontal wavenumbers $k_j(x, y)$ can be obtained from an acoustical spectral problem (we refer to [1] for details).

## 3. The Pseudo-differential Mode Parabolic Equation

In this section we deduce a pseudo-differential mode parabolic equation from the HRE (2). To do so, we start with the formal factorization of the operator in the HRE (2)

$$\left(\partial_x + \mathrm{i}\sqrt{k_j^2 + \partial_y^2}\right)\left(\partial_x - \mathrm{i}\sqrt{k_j^2 + \partial_y^2}\right) A_j = 0 \tag{3}$$

and focus on its solution consisting of the waves propagating in the positive direction of the $x$-axis, i.e. we consider

$$\left(\partial_x - \mathrm{i}\sqrt{k_j^2 + \partial_y^2}\right) A_j = 0\,. \tag{4}$$

Introducing the *reference modal eigenvalue* $k_{j,0}$ and cancelling out the principal oscillation from $A_j$

$$A_j(x, y) = e^{\mathrm{i}k_{j,0}x} \mathcal{A}_j(x, y)\,,$$

we obtain the *pseudo-differential mode parabolic equation (PDMPE)*

$$\frac{\partial \mathcal{A}_j}{\partial x} = \mathrm{i}k_{j,0}\Big(\sqrt{1+L_j}-1\Big)\,\mathcal{A}_j\,, \tag{5}$$

where $k_{j,0}^2 L_j = \partial_y^2 + k_j^2 - k_{j,0}^2$.

While the one-way Helmholtz equation (5) formulated in terms of the formal square-root Helmholtz operator, may be adequate for weakly range-dependent environments (if the number of wavelengths travelled is not too large), the inherently two-way (global) Helmholtz equation can be exactly reformulated, in a well-posed manner, in terms of one-way wave equations constructed in terms of appropriate Dirichlet-to-Neumann (DtN) operators [17, 18].

## 4. Numerical solution and approximations of PDMPE

The numerical solution of the PDMPE (5) usually follows one of the two approaches described in this section. In one of them (see §4.1 below) the square root operator $\sqrt{1+L_j}$ in the PDMPE (5) is replaced by a Padé approximation, and therefore the PDMPE turns into a wide-angle Padé MPE. The technique for its numerical solution is well-developed in the literature, and in the simplest case it can be considered as a generalization of the Crank-Nicholson method for the Schrödinger equation. The idea of this method was first outlined by Claerbout [19].

The second method, called *split-step Padé (SSP)*, combines the accuracy of higher-order Padé approximation with the efficiency of split-step approaches; it is based on the approximation of the propagator of the evolutionary equation (5) by a Padé series. This technique was first proposed by Collins [20] for the standard 2D PEs in underwater acoustics. It was also independently developed by Avilov [21]. For an application of the SSP method in conjunction with TBCs in electromagnetic wave propagation we refer the reader to [22].

Since both methods heavily rely on the Padé approximations of pseudo-differential operators, we start with its definition. Consider a function $F(\lambda)$

and its $(l,m)$-Padé approximant $\mathcal{R}(F,l,m)$

$$F(\lambda) \approx \mathcal{R}(F,l,m)(\lambda) \equiv \frac{P^F_{l,m}(\lambda)}{Q^F_{l,m}(\lambda)}\,, \tag{6}$$

where $P^F_{l,m}(\lambda)$ and $Q^F_{l,m}(\lambda)$ are the polynomials of degrees $l$ and $m$, respectively. Their coefficients can be easily computed from a linear system that is obtained by equating the rational function $P^F_{l,m}(\lambda)/Q^F_{l,m}(\lambda)$ to the truncated Taylor series of $F(\lambda)$ containing $l+m+1$ terms. A $(l,m)$-Padé approximant of a pseudo-differential operator $F(L)$ is formally defined as $P^F_{l,m}(L)/Q^F_{l,m}(L)$ (here $L$ is assumed to be a differential operator, e.g., $L_j$), cf. [23].

We remark that an alternative extremely effective and accurate rational operator approximation scheme for the square-root operator in the PDMPE (5) is what is commonly referred to as the *"rotated Padé" approximation* [24]. This approach is especially noteworthy for the relatively easy and accurate determination of the coefficients for very high order Padé approximation.

### *4.1. High-order Padé Mode Parabolic Equations*

Replacing the operator square root by its Padé approximant in the PDMPE (5) we obtain a high-order Padé MPE (or simply wide-angle MPE)

$$\frac{\partial \mathcal{A}_j}{\partial x} = \mathrm{i}k_{j,0}\left(\frac{P^F_{l,m}(L_j)}{Q^F_{l,m}(L_j)} - 1\right)\mathcal{A}_j\,. \tag{7}$$

The algorithm of the coefficients computation in Eq. (7) is based on the comparison of the Padé series with a truncated Taylor series. The details can be found in [25] (see also our MATLAB code). These coefficients can be also easily computed using a symbolic mathematical software, e.g. in the MAPLE software package the function call

```
l:=2; m:=2;
with(numapprox):pade(sqrt(1+Lj), Lj, [l,m]);
```

yields the desired values for the $(l,m)$-Padé approximant (6), cf. [26].

Now, the simplest way to solve wide-angle MPEs (WAMPEs) of the form (7) is to use the standard second-order Crank-Nicholson discretization along

the principal propagation direction (that is, in positive $x$-direction). Let us introduce a uniform grid $x_n = nh$ with the step $\Delta x = h$, and denote the values of $\mathcal{A}_j$ at the grid nodes as $\mathcal{A}_j^n \sim \mathcal{A}_j(x_n, y)$. Then, the WAMPE (7) can be discretized in $x$-dreiction as

$$D_h^+ \mathcal{A}_j^n = \mathrm{i}k_{j,0} \left( \frac{P_{l,m}^F(L_j)}{Q_{l,m}^F(L_j)} - 1 \right) \mathcal{A}_j^{n+1/2}, \tag{8}$$

where $F(\cdot) = \sqrt{\cdot}$,

$$D_h^+ \mathcal{A}^n = \frac{\mathcal{A}^{n+1} - \mathcal{A}^n}{h}, \qquad \mathcal{A}^{n+1/2} = \frac{\mathcal{A}^{n+1} + \mathcal{A}^n}{2}$$

denote the usual forward difference operator and the midpoint average (hereafter, for brevity, we always omit in the sequel the mode number subscript in discretized equations).

After some algebraic calculations the semi-discretized WAMPE (8) can be rewritten as

$$\mathcal{A}^{n+1} = \frac{U(L)}{W(L)} \mathcal{A}^n, \tag{9}$$

where

$$U(L) = \big(1 - \frac{\mathrm{i}k_0}{2} h\big) Q_{l,m}^F(L) + \frac{\mathrm{i}k_0}{2} h \, Q_{l,m}^F(L),$$
$$W(L) = \big(1 + \frac{\mathrm{i}k_0}{2} h\big) Q_{l,m}^F(L) - \frac{\mathrm{i}k_0}{2} h \, Q_{l,m}^F(L),$$

are the polynomials in $L$ of degree $p = \max(l, m)$. It is convenient to rewrite their ratio $U/W$ in Eq. (9) using a partial fraction expansion

$$\mathcal{A}^{n+1} = \left( 1 + \sum_{s=1}^{p} \frac{a_{l,m}^s L}{1 + b_{l,m}^s L} \right) \mathcal{A}^n. \tag{10}$$

This additive splitting form of equation (10) prevents powers of $L$ and hence it is convenient for a numerical implementation (discussed in the next Section 4.2) and suitable for parallel computing.

### *4.2. The SSP Solution Approach for the PDMPE*

Another approach proposed by Collins [20] to solve the one-way Helmholtz equations is called the split-step Padé (SSP) algorithm that also allows for a

powerful parallel implementation. Within this approach the Padé approximation and the marching of the field in range are interchanged, i.e., first the PDMPE (5) is formally advanced in range and then the Padé approximation is used for the respective propagator. On a small interval of length $\Delta x = h$ the PDMPE (5) can be formally solved as

$$\mathcal{A}^{n+1} = \exp\Big(\mathrm{i}k_{j,0}h\big(\sqrt{1+L}-1\big)\Big)\mathcal{A}^{n}\,. \tag{11}$$

A $(l,m)$-Padé approximant of the exponential on the right-hand side of the latter formula (knows as the propagator) can be written in the form of a partial fraction expansion as

$$\exp\Big(\mathrm{i}k_{j,0}h\big(\sqrt{1+L}-1\big)\Big) \approx \frac{\tilde{U}(L)}{\tilde{W}(L)} = \left(1+\sum_{s=1}^{p}\frac{\tilde{a}_{l,m}^{s}L}{1+\tilde{b}_{l,m}^{s}L}\right), \tag{12}$$

and hence the solution of the PDMPE (5) can be advanced in $x$-direction by

$$\mathcal{A}^{n+1} = \left(1+\sum_{s=1}^{p}\frac{\tilde{a}_{l,m}^{s}L}{1+\tilde{b}_{l,m}^{s}L}\right)\mathcal{A}^{n}\,. \tag{13}$$

Clearly, the polynomials $\tilde{U}(\lambda)$ and $\tilde{W}(\lambda)$ in Eq. (13) are different from $U(\lambda)$ and $W(\lambda)$ in Eq. (9). The coefficients $a_{l,m}^{s}$, $b_{l,m}^{s}$ and $\tilde{a}_{l,m}^{s}$, $\tilde{b}_{l,m}^{s}$ from their respective partial fraction expansions are different as well (we emphasize this fact by tildes over the latter ones). At the same time, the marching schemes (9) and (13) are obviously very similar, and they can be advanced in $x$-direction by the same simple method described below (hereafter we omit the tildes keeping in mind that all discussed techniques are applicable to both forms).

We note that the computation of the coefficients $a_{l,m}^{s}$, $b_{l,m}^{s}$ is described in [25], and we do not reproduce the details here (clearly, it is very close to the standard partial fraction expansion method). It is also important to note that although in many cases the choice $l = m$ works fairly well, an additional accuracy for the treatment of evanescent modes can be gained by using the so-called $\theta$-propagator approach [27, 25]. Within this approach, the approximant $\tilde{U}/\tilde{W}$ in Eq. (12) is the weighted combination of the Padé expansions with $l = m$ and $l = m-1$ (with weights $\theta$ and $1-\theta$, respectively).

A very useful implementation of SSP approach for the simulation of radiowaves propagation is described in a recent paper [28].

*4.3. The Finite-difference Discretization of L*

Let us now introduce, for simplicity only, a uniform grid $y_q = q\delta$ with step size $\Delta y = \delta$ in the transverse direction and replace the second derivative in $L$ by its standard finite-difference counterpart

$$D_\delta^2 \mathcal{A}^{n+1,q} = \frac{\mathcal{A}^{n+1,q+1} - 2\mathcal{A}^{n+1,q} + \mathcal{A}^{n+1,q-1}}{\delta^2}\,, \qquad q \in \mathbb{Z},$$

where $\mathcal{A}^{n,q} \sim \mathcal{A}(x_n, y_q)$. Then both Eq. (13) and Eq. (9) turn into a fully discretized marching scheme of the additive form

$$\mathcal{A}^{n+1,q} = \left(1 + \sum_{s=1}^{p} \frac{a_{l,m}^s L_\delta}{1 + b_{l,m}^s L_\delta}\right) \mathcal{A}^{n,q}\,, \qquad q \in \mathbb{Z}, \tag{14}$$

where $k_0^2 L_\delta = D_\delta^2 + k^2 - k_0^2$.

Next, we introduce the intermediate functions $\mathcal{B}_1^{n+1,q}, \ldots, \mathcal{B}_{p-1}^{n+1,q}$ such that

$$(1 + b_{l,m}^s L_\delta)\, \mathcal{B}_s^{n+1,q} = a_{l,m}^s\, L_\delta \mathcal{A}^{n,q}\,, \qquad s = 1, 2, \ldots, p-1, \tag{15}$$

and separately for $s = p$

$$(1 + b_{l,m}^p L_\delta)\, \mathcal{B}_p^{n+1,q} = \mathcal{A}^{n,q} + (b_{l,m}^p + a_{l,m}^p)\, L_\delta \mathcal{A}^{n,q}\,. \tag{16}$$

Here, $\mathcal{B}_s^{n,q}$, $s = 1, 2, \ldots, p$, can be computed efficiently by inverting tridiagonal matrices $(1 + b_{l,m}^s L_\delta)$. Thus we arrive finally at the following system

$$\mathcal{A}^{n+1,q} = \sum_{s=1}^{p} \mathcal{B}_s^{n+1,q}, \qquad q \in \mathbb{Z}. \tag{17}$$

*4.4. The SSP Solution Approach for the discretized operator $L_\delta$*

Here we briefly review an idea of Collins [20] who showed how to modifiy the split-step Padé approach of Section 4.2 for the discretized operator $L_\delta$. A Taylor series yields formally

$$\mathcal{A}^n(y_{q\pm1}) = \exp(\pm\delta\partial_y)\mathcal{A}^n(y_q) = \exp\big(\pm\delta k_0(\sqrt{L - (k/k_0 - 1)}\big)\mathcal{A}^n(y_q)$$

and for simplicity we set $k = k_0$ and obtain the expression

$$L_\delta = -k_0^{-2}\frac{e^{\delta k_0\sqrt{L}} - 2 + e^{-\delta k_0\sqrt{L}}}{\delta^2} = -2\frac{\cosh\big(\tau\sqrt{L}\big) - 1}{\tau^2}, \quad \tau = \delta k_0, \tag{18}$$

which is well-known from the classical von-Neumann stability analysis. Now solving equation (18) for $L$ yields $L$ as a function of $L_\delta$:

$$L = \Gamma(L_\delta) = \tau^{-2}\log^2\Big[1 - \frac{\tau^2}{2}L_\delta + \sqrt{\big(1 - \frac{\tau^2}{2}L_\delta\big)^2 - 1}\Big], \tag{19}$$

and thus we have

$$\mathcal{A}^{n+1,q} = \exp\Big(\mathrm{i}k_0 h\big(\sqrt{1+\Gamma(L_\delta)} - 1\big)\Big)\,\mathcal{A}^{n,q}, \qquad n > 0. \tag{20}$$

We proceed analogously to (12) and apply the Padé approximation

$$\exp\Big\{ik_0 h\big(\sqrt{1+\Gamma(L_\delta)} - 1\big)\Big\} \approx 1 + \sum_{s=1}^{p}\frac{\tilde{a}^s_{l,m}L_\delta}{1 + \tilde{b}^s_{l,m}L_\delta}. \tag{21}$$

Finally, inserting (21) into (20) we get the marching scheme

$$\mathcal{A}^{n+1,q} = \mathcal{A}^{n,q} + \sum_{s=1}^{p}\frac{\tilde{a}^s_{l,m}L_\delta}{1 + \tilde{b}^s_{l,m}L_\delta}\,\mathcal{A}^{n,q}, \qquad n > 0. \tag{22}$$

## 5. Artificial truncation of the computational domain

In practical problems of underwater acoustics the computational domain is usually unbounded in the transverse direction to the acoustical track of interest. Indeed, it represents an area of the sea with no physical walls at $y = y_0$ and $y = y_Q$. Thus, in general it is necessary to suppress the reflections of waves at these artificial boundaries. There exist two main approaches for handling this issue. In the first approach the domain is extended by two layers that absorb outgoing waves (one on each side of the domain where the solution in sought). The second approach consists in designing the artificial boundary conditions of a special kind that couple the solution in the domain of interest to the outgoing-wave solution in the outer halfspace. Both methods have certain strengths and weaknesses, and we discuss them in detail in the remainder of this section.

It is important to note that all domain truncation methods considered here require that the medium outside the computational domain is homogeneous. Of course, this is not a realistic requirement for the real ocean, and in practice we simply have to choose the domain is such a way that the inhomogeneities outside it do not affect the solution. For an artificial boundary condition for an elastic sea bootom we refer the interested reader to [29].

### *5.1. Perfectly matching layers*

In 1994 the perfectly matched layer method (PML) was pioneered by Bérenger [30] for Maxwell's equations and Chew and Weedon [31] showed that the PML can be regarded as a complex coordinate stretching. In the sequel, Levy [32] adapted the PML method to parabolic wave equation models. Later in 2007, Lu and Zhu [33] showed the effectiveness of computing an underwater acoustic benchmark wedge problem with operator rational approximations to the one–way Helmholtz equation and a PML of 1/4 wavelength thickness.

Let us note that a brief construction of the PML for the Schrödinger equation can be found in [34, Section 3.3] and this method is outlined in [35, Section 3.5]

Assume that the solution of Eq. (5) is sought on the domain $(x, y) \in \Omega = [0, x_{max}] \times [y_0, y_Q]$. We increase the width of this stripe by $\varepsilon$ from each side and consider an initial-value problem for Eq. (5) on the extended domain $\bar{\Omega} = [0, x_{max}] \times [-y_0 - \varepsilon, y_Q + \varepsilon]$, where the operator $L$ is replaced by $L_{PML}$ defined as

$$k_0^2 L_{PML} = \frac{1}{1 + \mathrm{i}\beta(y)} \frac{\partial}{\partial y} \frac{1}{1 + \mathrm{i}\beta(y)} \frac{\partial}{\partial y} + k^2 - k_0^2 \,,$$

for a smooth function $\beta(y)$ which is increasing in $y$ on $[y_Q, y_Q + \varepsilon]$, decreasing on $[y_0 - \varepsilon, y_0]$, and such that $\beta(y) = 0$ for $y \in [y_0, y_Q]$. Thus, the operator $L_{PML}$ coincides on $[-y_0, y_Q]$ with $L$, and outside this interval the derivatives $\frac{\partial}{\partial y}$ in $L$ are replaced by $\frac{1}{1+\mathrm{i}\beta(y)} \frac{\partial}{\partial y}$.

Our numerical scheme implements the solution of an initial-boundary value problem for Eq. (5) on the domain $\bar{\Omega}$ with homogeneous Dirichlet boundary conditions of the form $\mathcal{A}|_{y=y_0-\varepsilon} = \mathcal{A}|_{y=y_Q+\varepsilon} = 0$ at the boundaries $y = y_0 - \varepsilon$ and $y = y_Q + \varepsilon$ of the PMLs. Inside the domain $\Omega$, this solution accurately

approximates the solution of Eq. (5) on the unbounded domain $-\infty < y < \infty, x \geq 0$ provided that $\beta(y)$ increases sufficiently smoothly from zero to its maximal value as we move deeper into the PML. In the examples presented later in this study, we set $\beta(y) = \beta_0(y - y_Q)^3/\varepsilon^3$ (with $\beta_0 = 5$, $\varepsilon = 300$ m).

It is also important that the replacement of the operator $L$ with its PML counterpart $L_{PML}$ is equivalent to the following coordinates transformation

$$\tilde{y} = y + \mathrm{i} \int_0^y \beta(y)\, dy\,. \tag{23}$$

This property is used later for matching the PML with the non-localized initial conditions, see Eq. (36).

### *5.2. Transparent boundary conditions*

Specific boundary conditions that suppress wave reflection at an artificial boundary are called *transparent boundary conditions* (TBCs). They were first independently developed by Baskakov and Popov [36] and Papadakis [37] for narrow-angle parabolic equation. Later on, Popov was also first to derive TBCs for simplest wide-angle PEs [38]. In all these pioneering works TBCs were obtained in the continuous form.

While such TBCs fully solve the problem of cutting off the horizontal $y$-domain for the differential equation, their adequate numerical discretization is far from trivial [39]. In fact, all available discretizations are less accurate than the discretized half-space problem and they render the overall numerical scheme only conditionally stable [40, 41]. Papadakis [37] derived in 1994 a TBC for the one-way Helmholtz equation that was later (in a similar formulation) implemented by Brooke and Thomson [42] and exposed computational instabilities. Also in 2000, [43] Friese, Schmidt and Yevick proposed semi-discrete TBCs for a fourth-order wide-angle approximation of the two-dimensional Helmholtz equation that yielded an unconditionally stable propagation method. This approach, being discrete in the propagation direction, was later generalized in [44] for arbitrary Padé approximations.

Fully-discrete TBCs for narrow-angle PEs were developed by Arnold and Ehrhardt [39] (see also a review article [35]). These TBCs fully eliminate spurious reflections at artificial boundaries and lead to the unconditionally stable numerical scheme Later the theory was also extended to wide-angle Padé PEs in [45, 46, 26, 47].

Here we construct and analyze the discrete transparent boundary conditions (TBCs) for the split-step Padé algorithm for the PDMPE. The discrete TBCs are obtained by $\mathcal{Z}$–transformation of the numerical schemes for $q \le 0$ or $q \ge Q$.

In the sequel we make the basic assumption that the initial data $\mathcal{A}^0 \sim \mathcal{A}(0,y)$, is confined in the computational domain $y_0 < y < y_Q$, i.e. $\operatorname{supp}\mathcal{A}(0,y) \subset (y_0, y_Q)$. Approaches to overcome this restriction, e.g. when using the self-starter (see §6.2) can be found in [48, 46].

We consider the system (15)–(16)

$$
\begin{aligned}
a^s_{l,m}\, L_\delta \mathcal{A}^{n,q} - b^s_{l,m}\, L_\delta \mathcal{B}^{n+1,q}_s &= \mathcal{B}^{n+1,q}_s\,, \quad s = 1,2,\ldots,p-1,\\
(b^p_{l,m} + a^p_{l,m})\, L_\delta \mathcal{A}^{n,q} - b^p_{l,m}\, L_\delta\, \mathcal{B}^{n+1,q}_p &= \mathcal{B}^{n+1,q}_p - \mathcal{A}^{n,q}.
\end{aligned}
$$

and recalling that $k_0^2 L_\delta = D_\delta^2 + k^2 - k_0^2$ we arrive at

$$
\begin{aligned}
a^s_{l,m}\, D^2_\delta \mathcal{A}^{n,q} - b^s_{l,m}\, D^2_\delta \mathcal{B}^{n+1,q}_s&\\
= k_0^2 \mathcal{B}^{n+1,q}_s + b^s_{l,m}(k^2 - k_0^2)\, \mathcal{B}^{n+1,q}_s - a^s_{l,m}(k^2 - k_0^2)\, \mathcal{A}^{n,q}&
\end{aligned}
$$

for $s = 1,2,\ldots,p-1$ and

$$
\begin{aligned}
&(b^p_{l,m} + a^p_{l,m})\, D^2_\delta \mathcal{A}^{n,q} - b^p_{l,m} D^2_\delta\, \mathcal{B}^{n+1,q}_p\\
&= k_0^2 \mathcal{B}^{n+1,q}_p - k_0^2 \mathcal{A}^{n,q} + b^p_{l,m}(k^2 - k_0^2)\, \mathcal{B}^{n+1,q}_p - (b^p_{l,m} + a^p_{l,m})(k^2 - k_0^2)\, \mathcal{A}^{n,q}.
\end{aligned}
$$

Without loss of generality we focus on the case of the right discrete TBC at $q = Q$. To solve this system we use the *$\mathcal{Z}$-transformation* with respect to $x$

$$
\mathcal{Z}\{\mathcal{A}^{n,q}\} = \hat{\mathcal{A}}^q(\zeta) := \sum_{n=0}^{\infty} \zeta^{-n} \mathcal{A}^{n,q}, \quad \zeta \in \mathbb{C}, \quad |\zeta| > R_{\hat{\mathcal{A}}^q}, \tag{24}
$$

where $R_{\hat{\mathcal{A}}^q}$ denotes the convergence radius of this Laurent series. Note that we denoted in (24) the transformation variable with $\zeta$ in order keep $z$ for the

depth variable. We apply the $\mathcal{Z}$-transformation (24) which yields the following $\mathcal{Z}$-transformed system for the right exterior problem $q \geq Q$

$$a^s_{l,m}\, D^2_\delta \hat{\mathcal{A}}^q - \zeta b^s_{l,m}\, D^2_\delta \hat{\mathcal{B}}^q_s = \zeta h k_0^2 \hat{\mathcal{B}}^q_s + \zeta b^s_{l,m}(k^2 - k_0^2)\, \hat{\mathcal{B}}^q_s - a^s_{l,m}(k^2 - k_0^2)\, \hat{\mathcal{A}}^q$$

for $s = 1, 2, \ldots, p-1$ and

$$\begin{aligned}(b^p_{l,m} + a^p_{l,m})\, D^2_\delta \hat{\mathcal{A}}^q - \zeta b^p_{l,m} D^2_\delta\, \hat{\mathcal{B}}^q_p \\ = \zeta k_0^2 \hat{\mathcal{B}}^q_p - k_0^2 \hat{\mathcal{A}}^q + \zeta b^p_{l,m}(k^2 - k_0^2)\, \hat{\mathcal{B}}^q_p - (b^p_{l,m} + a^p_{l,m})(k^2 - k_0^2)\, \hat{\mathcal{A}}^q.\end{aligned}$$

We rewrite this transformed system above in matrix notation as

$$\mathbf{X} D^2_\delta \hat{\boldsymbol{\psi}}_q = \mathbf{Y} \hat{\boldsymbol{\psi}}_q, \qquad q \geq Q, \tag{25}$$

where we defined the vector $\hat{\boldsymbol{\psi}}_q = (\hat{\mathcal{A}}^q, \hat{\mathcal{B}}^q_1, \ldots, \hat{\mathcal{B}}^q_p)^\top \in \mathbb{C}^{p+1}$ and the complex $(p+1) \times (p+1)$-matrices

$$\mathbf{X} := \begin{pmatrix} a^1_{l,m} & -\zeta b^1_{l,m} & & \\ \vdots & & \ddots & \\ a^{p-1}_{l,m} & & & -\zeta b^{p-1}_{l,m} \\ b^p_{l,m} + a^p_{l,m} & \cdots & \cdots & -\zeta b^p_{l,m} \end{pmatrix}$$

and

$$\mathbf{Y} := \begin{pmatrix} -a^1_{l,m}(k^2-k_0^2) & \zeta h k_0^2 + \zeta b^1_{l,m}(k^2-k_0^2) & & \\ \vdots & & \ddots & \\ -a^{p-1}_{l,m}(k^2-k_0^2) & & & \zeta h k_0^2 + \zeta b^{p-1}_{l,m}(k^2-k_0^2) \\ -k_0^2 - (b^p_{l,m} + a^p_{l,m})(k^2-k_0^2) & & & \zeta k_0^2 + \zeta b^p_{l,m}(k^2-k_0^2) \end{pmatrix}.$$

The remaining part of the construction follows [26]. By introducing $\hat{\boldsymbol{\xi}}_q := \Delta_h^- \hat{\boldsymbol{\psi}}_q$ we rewrite (25) as a system of $2(p+1)$ first order difference equations

$$\underbrace{\begin{pmatrix} \mathbf{0} & \mathbf{X} \\ \mathbf{I} & -\mathbf{I} \end{pmatrix}}_{\mathbf{A}} \Delta_h^+ \begin{pmatrix} \hat{\boldsymbol{\psi}}_q \\ \hat{\boldsymbol{\xi}}_q \end{pmatrix} = \underbrace{\begin{pmatrix} \mathbf{Y} & \mathbf{0} \\ \mathbf{0} & \mathbf{I} \end{pmatrix}}_{\mathbf{B}} \begin{pmatrix} \hat{\boldsymbol{\psi}}_q \\ \hat{\boldsymbol{\xi}}_q \end{pmatrix},$$

i.e.

$$\begin{pmatrix}\Delta_h^+\hat{\boldsymbol{\psi}}_q\\ \Delta_h^+\hat{\boldsymbol{\xi}}_q\end{pmatrix} = \mathbf{A}^{-1}\mathbf{B}\begin{pmatrix}\hat{\boldsymbol{\psi}}_q\\ \hat{\boldsymbol{\xi}}_q\end{pmatrix} \quad \text{or} \quad \begin{pmatrix}\hat{\boldsymbol{\psi}}_{q+1}\\ \hat{\boldsymbol{\xi}}_{q+1}\end{pmatrix} = (\mathbf{A}^{-1}\mathbf{B}+\mathbf{I})\begin{pmatrix}\hat{\boldsymbol{\psi}}_q\\ \hat{\boldsymbol{\xi}}_q\end{pmatrix}, \quad q \geq Q\,.$$

We split the Jordan form $\mathbf{J} = \mathrm{diag}(\mathbf{J}_1, \mathbf{J}_2)$ of $\mathbf{A}^{-1}\mathbf{B}+\mathbf{I}$ , $\mathbf{J}_1 \in \mathbb{C}^{(p+1)\times(p+1)}$ containing the Jordan blocks corresponding to solutions decaying for $q \to \infty$ and $\mathbf{J}_2 \in \mathbb{C}^{(p+1)\times(p+1)}$ those which increase. With the matrix of left eigenvectors $\mathbf{P}^{-1} = \left(\begin{smallmatrix}\mathbf{P}_1 & \mathbf{P}_2\\ \mathbf{P}_3 & \mathbf{P}_4\end{smallmatrix}\right)$ the equation

$$\begin{aligned}\mathbf{P}^{-1}\begin{pmatrix}\hat{\boldsymbol{\psi}}_{q+1}\\ \hat{\boldsymbol{\xi}}_{q+1}\end{pmatrix} &= \mathbf{P}^{-1}(\mathbf{A}^{-1}\mathbf{B}+\mathbf{I})\begin{pmatrix}\hat{\boldsymbol{\psi}}_q\\ \hat{\boldsymbol{\xi}}_q\end{pmatrix} = \mathbf{P}^{-1}\mathbf{P}\begin{pmatrix}\mathbf{J}_1 & \mathbf{0}\\ \mathbf{0} & \mathbf{J}_2\end{pmatrix}\begin{pmatrix}\mathbf{P}_1 & \mathbf{P}_2\\ \mathbf{P}_3 & \mathbf{P}_4\end{pmatrix}\begin{pmatrix}\hat{\boldsymbol{\psi}}_q\\ \hat{\boldsymbol{\xi}}_q\end{pmatrix}\\ &= \begin{pmatrix}\mathbf{J}_1 & \mathbf{0}\\ \mathbf{0} & \mathbf{J}_2\end{pmatrix}\begin{pmatrix}\mathbf{P}_1\hat{\boldsymbol{\psi}}_q + \mathbf{P}_2\hat{\boldsymbol{\xi}}_q\\ \mathbf{P}_3\hat{\boldsymbol{\psi}}_q + \mathbf{P}_4\hat{\boldsymbol{\xi}}_q\end{pmatrix}\end{aligned}$$

holds and thus the *transformed right discrete TBC* reads

$$\mathbf{P}_3\hat{\boldsymbol{\psi}}_Q + \mathbf{P}_4\hat{\boldsymbol{\xi}}_Q = 0.$$

For a regular matrix $\mathbf{P}_4$ the $\mathcal{Z}$–transformed right discrete TBC can be written in DtN form

$$\Delta_h^-\hat{\boldsymbol{\psi}}_Q = \widehat{\mathbf{D}}\hat{\boldsymbol{\psi}}_Q\,,$$

where $\widehat{\mathbf{D}} = -(\mathbf{P}_4)^{-1}\mathbf{P}_3$. Finally, an inverse $\mathcal{Z}$-transformation yields the discrete right *TBC*

$$\boldsymbol{\psi}_Q^{n+1} - \boldsymbol{\psi}_{Q-1}^{n+1} - \mathbf{D}^0\boldsymbol{\psi}_Q^{n+1} = \sum_{l=1}^{n}\mathbf{D}^{n+1-l}\boldsymbol{\psi}_Q^l\,. \tag{26}$$

for the vector $\boldsymbol{\psi}_q^n = (\mathcal{A}^{n,q}, \mathcal{B}_1^{n,q}, \ldots, \mathcal{B}_p^{n,q})^\top \in \mathbb{C}^{p+1}$, $q = Q-1, Q$, with the convolution coefficients given by the Cauchy integral formula

$$\mathbf{D}^n = \mathcal{Z}^{-1}\{\widehat{\mathbf{D}}(z)\} = \frac{\tau^n}{2\pi}\int_0^{2\pi}\widehat{\mathbf{D}}(\tau e^{i\varphi})e^{in\varphi}\,d\varphi, \quad n \in \mathbb{Z}_0, \quad \tau > 0.$$

Since this inverse $\mathcal{Z}$-transformation cannot be done explicitly, we use a numerical inversion technique based on FFT (cf. [49]); details of this routine (especially the choice of the inversion radius $\tau$) can be found in [50]; see also [47] for another inversion approach.

## 6. Initial conditions for WAMPEs

In this section we describe starters (Cauchy data) that can be used to initialize the solution of a WAMPE at $x = 0$. In underwater acoustics starters are usually constructed in such a way that the resulting WAMPE solution approximates the field produced by a point source. Technically, the approaches for initializing standard wide-angle PEs (see, e.g., [1]) can be also used for MPEs, with the exception of modal starters. In this section we discuss advantages and shortcomings of different initial conditions (ICs) for WAMPEs.

### *6.1. Greene's starter*

The Greene's starter originally developed for a rational-linear Padé PE [1, 51] is probably the simplest initial condition for WAMPEs to implement. For equation

$$\frac{\partial \mathcal{A}_j}{\partial x} = ik_{j,0}\,\frac{\alpha_0 + \alpha_1 L_j}{1 + cL_j}\,\mathcal{A}_j\,. \tag{27}$$

it is given by the formula

$$\mathcal{A}_j(0, y) = \frac{\varphi_j(z_s)}{2\sqrt{\pi}}\big(1.4467 - 0.8402k_{j,0}^2 y^2\big)\,e^{-\frac{k_{j,0}^2 y^2}{1.5256}}\,. \tag{28}$$

It provides sufficient aperture to solve most practical problems of underwater acoustics. Obviously, it is strongly localized in a relatively small vicinity of $y = 0$, and therefore it can be easily used both with PMLs and TBCs. On the other hand, it also sets a restriction on the grid steps in both $x$ and $y$ direction. If the step size $\delta$ is too large, then the starter is not smooth enough, and the resulting oscillations can spoil the solution. We found that 15 points per half-period of the horizontal wavelength $2\pi/k_{j,0}$ is usually sufficient to obtain an accurate solution, and therefore $15k_{j,0}\delta < \pi$ (i.e., $\delta$ should be less that $|0.2/k_{j,0}|$).

Although in principle high-order Padé MPEs admit much larger steps $h$ in range $x$ than required by the usual wavelength-based rule (e.g., 10–20 points per wavelength), and they can be even larger in the SSP method, the starter (28) poses additional restriction on the value of $h$ due to the non-physical oscillations in its sidelobes.

*6.2. Self-starter*

The self-starter approach was originally developed 1992 by Collins [52]. It can be used both for wide-angle PEs and in the SSP solution procedure. In this subsection we show how this self-starter can be used with MPEs and explain how it can be combined with PMLs.

In the description of the self-starter it is more convenient to use Eq. (5) that can be also rewritten as

$$\partial_x A = \mathrm{i}k_0\big(\sqrt{1+L}-1\big)\,A\,, \tag{29}$$

where we again omit the subscript $j$ numbering the vertical modes. Let us assume for the moment that the medium properties in Eq. (5) are independent on $x$, i.e., that $k = k(y)$.

Consider a complete system of eigenfunctions $\{f_\nu(y)\}$ of the operator $\partial_y^2 + k^2$ on the interval $(-\infty, \infty)$ with their respective eigenvalues $\lambda_\nu^2$. The solution of the horizontal refraction equation (2) for $x > 0$ in this case can be written as

$$A(x,y) = \frac{\mathrm{i}\varphi(z_s)}{2}\int \frac{1}{\lambda_\nu} f_\nu(0) f_\nu(y)\,\mathrm{e}^{\mathrm{i}\lambda_\nu x}\,d\nu\,. \tag{30}$$

It can be easily seen that the solution (30) at $x = 0$ reduces to the function

$$A_0(y) \equiv A(0,y) = \frac{\mathrm{i}\varphi(z_s)}{2}\int \frac{1}{\lambda_\nu} f_\nu(0) f_\nu(y)\,d\nu\,,$$

that satisfies a one-dimensional boundary-value problem (BVP) for the equation

$$\sqrt{\partial_y^2 + k^2}\,A_0 = \frac{\mathrm{i}\varphi(z_s)}{2}\,\delta(y)$$

with the radiation boundary conditions at infinity. This BVP does not admit direct numerical solution $k = k(y)$. Instead, indirect approach of Collins [52] can be adapted to the case of MPEs. The algorithm consists of three steps, and the first one is the solution of an auxiliary BVP

$$(1+L)\Phi = \frac{\mathrm{i}\varphi(z_s)}{2k_0^2}\,\delta(y)\,, \tag{31}$$

that can be easily obtained numerically (using matching conditions for the delta function $\delta(y)$ at $y = 0$). In the case of constant $k(y) = k_0$, the BVP (31)

possesses a simple analytical solution

$$\Phi_0(y) = \frac{\varphi(z_s)}{4}\, \mathrm{e}^{\mathrm{i}k_0|y|}\,, \tag{32}$$

with the discontinuous derivative at $y = 0$. In the case of arbitrary $k(y)$ the solution of (31) can be expressed in terms of eigenfunctions $\{f_\nu(y)\}$

$$\Phi_0(y) = \frac{\mathrm{i}\varphi(z_s)}{2} \int \frac{1}{\lambda_\nu^2} f_\nu(0) f_\nu(y) d\nu\, \delta(y)\,. \tag{33}$$

The second step consists in advancing $\Phi(y)$ short range to $x = x_0$ using either the scheme (10) or its SSP counterpart (13). As a result, we obtain

$$\Phi_{x_0}(y) = \frac{\mathrm{i}\varphi(z_s)}{2} \int \frac{1}{\lambda_\nu^2} \mathrm{e}^{\mathrm{i}\lambda_\nu x_0} f_\nu(0) f_\nu(y) d\nu\, \delta(y)\,. \tag{34}$$

From Eq. (30) it is clear, that modal amplitude $A(x_0, y)$ can be computed from $\Phi_{x_0}(y)$ by applying the operator $k_0\sqrt{1+L}$, i.e.,

$$A(x_0, y) = k_0\sqrt{1+L}\Phi_{x_0}(y)\,.$$

At this point the operator $\sqrt{1+L}$ can be replaced by its Padé approximation (in a product form)

$$\sqrt{1+L} = \prod_{s=1}^{p} \frac{1 + c^s L}{1 + b^s L}\,. \tag{35}$$

Using the operator approximation in Eq. (35) we can easily compute $A(x_0, y)$ from $\Phi_{x_0}(y)$ and use it as a starter for a WAMPE at $x = x_0$.

Although this approach allows to set up a starter with arbitrarily large angular aperture in the horizontal plane, it also brings some spurious oscillations into the numerical solutions since advancing of $\Phi_0$ to the range $x = x_0$ involves the computation of its second derivative with respect to $y$ (and even its first derivative is not continuous). However, self-starter works reasonably well provided that the the steps $h$ and $\delta$ are sufficiently small (see examples in §7).

Let us also note, that the initial condition at $x = 0$ obtained from the BVP (31) does not have compact support. This is also clear from Eq. (32). Thus, it is inefficient to use it in a combination with the TBCs, and the PML option

should be chosen for this type of starter. The coordinate transformation (23) allows us to adapt Eq. (32) for a solver with PMLs, e.g., for $y > 0$ we have

$$\Phi_0(y) = \frac{\varphi(z_s)}{4}\,\mathrm{e}^{\mathrm{i}k_0 y}\mathrm{e}^{-k_0\int_0^y \beta(y)dy}\,, \tag{36}$$

where the last factor is responsible for the decay of $\Phi_0(y)$ inside the PMLs. Since the numerical solution of the BVP (31) must also start with an analytical computation of $\Phi_0(y)$ on the intervals $[y_0 - \varepsilon, y_0]$ and $[y_Q, y_Q + \varepsilon]$, it is not difficult to extend the correction associated with PML to this case.

For the cubic PML attenuation profile from §5.1 Eq. (36) turns into

$$\Phi_0(y) = \frac{\varphi(z_s)}{4}\,\mathrm{e}^{\mathrm{i}k_0 y}\mathrm{e}^{-\frac{k_0\beta_0}{4\varepsilon^3}(y-y_Q)^4} \tag{37}$$

for $y > y_Q$.

*6.3. A ray-based starter for WAMPEs*

In this subsection we propose a new starter for WAMPEs (that can be also used for standard PEs) which is based on the ray theory. The very idea is very simple and natural for the considered problem setting, as the computational domains for MPEs are typically unbounded in $y$ (by contrast to the case of standard PEs solved in $r, z$ coordinates on the domain which is typically bounded in $z$). For such domains and slowly varying environmental parameters the ray-theoretical solution is highly accurate and easy to compute. One might argue that the need in PEs is questionable when the ray theory can be successfully applied. In our opinion, however, in practical problems PEs offers more advantages due to their robustness and their omnivorous nature. The solution algorithms for PEs are straightforward, and typical issues that cripple any ray-based code, including eigenray identification problems, caustics and ray chaos, never emerge. All these difficulties however can be ignored when computing the ray solution at ranges of several tens of meters from the source.

Assume that for $x < x_0$ (where $x_0$ is comparable to the wavelength) the medium properties do not depend on $x$, i.e., $k = k(y)$. The ray-theoretical representation [1] of the solution of Eq. (2) has the form

$$A(x, y) = M(x, y)\mathrm{e}^{\mathrm{i}k_0 S(x,y)} + o(1/k_0)\,, \tag{38}$$

where $M(x,y)$ in the zeroth-order amplitude and $S(x,y)$ is the phase (this is an asymptotic of the exact solution for large $k_0$). The phase $S$ satisfies the Hamilton-Jacobi equation

$$(\partial_x S)^2 + (\partial_y S)^2 = n(x,y)\,, \tag{39}$$

where $n(x,y) \equiv k(x,y)/k_0$ is the horizontal refractive index. After solving (39) the amplitude $M$ can be obtained from the transfer equation of the form

$$2(\partial_x S \partial_x M + \partial_y S \partial_y M) + (\partial_x^2 S + \partial_y^2 S)M = 0\,. \tag{40}$$

Both Eq. (39) and Eq. (40) can be solved along the characteristics determined from the Hamiltonian system

$$\begin{aligned} \frac{dx}{d\ell} &= \frac{1}{n}\xi\,, \qquad & \frac{d\xi}{d\ell} &= \partial_x n\,, \\ \frac{dy}{d\ell} &= \frac{1}{n}\eta\,, \qquad & \frac{d\eta}{d\ell} &= \partial_y n\,, \end{aligned} \tag{41}$$

where $\ell$ denotes a natural parameter (i.e., the arclength along the characteristics), and $\xi, \eta$ are conjugate variables to $(x,y)$ (the momenta). The projections of the characteristics (41) onto the coordinate plane $(x,y)$ are called horizontal rays corresponding to the vertical mode under consideration (the one for which we are computing the amplitude $A = A_j$). Let us note that the ray-theoretical representation of modal amplitudes was first used by Burridge and Weinberg [2]. The initial condition for the system (41) reads

$$\begin{aligned} x(0) &= 0\,, \quad & \xi(0) &= \cos\alpha\,, \\ y(0) &= 0\,, \quad & \eta(0) &= \sin\alpha\,, \end{aligned} \tag{42}$$

where the the rays family is parametrized by the take-off angle $\alpha$.

After solving Eq. (41) we can compute the phase along the rays as

$$S(\ell) = S(0) + \int_0^\ell n(\ell)\, d\ell.$$

The amplitude $M(\ell)$ in the case $n = n(y)$ can be expressed as

$$M(\ell) = \frac{M_0}{n(\ell)} \sqrt{\frac{\cos\alpha}{\partial y(\ell,\alpha)/\partial\alpha}}\,, \tag{43}$$

where $M_0$ denotes the amplitude at 1m from the source.

Since we need the ray-based solution only for small values of $x < x_0$, in most cases the starter is accurate enough even if we use the rays computed for a horizontally homogeneous medium with $k(x, y) = k_0$ ($n = 1$). In this case we have

$$x(\ell) = \ell \cos\alpha\,, \quad y(\ell) = \ell \sin\alpha\,, \quad S(\ell) = \ell\,, \quad M(\ell) = \frac{M_0}{\sqrt{r}}\,, \tag{44}$$

where $M_0 = \mathrm{e}^{\mathrm{i}\pi/4}/\sqrt{8\pi k_0}$ (the amplitude normalisation factor $M_0$ is chosen to fit the analytical solution of Eq. (2) in the homogeneous medium). Obviously, the ray-based starter can also be used for standard PEs involving the $z$ coordinate (including 3D PEs). However this approach should be done carefully, especially in the low-frequency regime (when the wavelength is comparable with the water depth), and in most cases the numerical solution of the system (41) will be required.

For a ray-based starter one can explicitly specify the required aperture by suitably defining the interval of the values of the take-off angle $\alpha$. Outside the interval a tapering function should be used for the amplitudes in order to make the starter smooth.

## 7. Numerical Examples

In this section we present a collection of computational examples that illustrate the accuracy of the WAMPE-based computational model in various propagation scenarios of shallow-water acoustics. In the first example we consider the Pekeris waveguide (i.e., the one with flat horizontal bottom) in order to illustrate the capabilities of the three starters discussed above (see §6). In the second example we handle a standard 3D wedge problem which is routinely used for the validation of 3D sound propagation models. In the third example we study the problem where the acoustical field is focused by an underwater canyon.

### 7.1. Shallow-water waveguide with flat bottom: different starters

In the first example we consider the sound propagation in a shallow-water waveguide with a flat horizontal bottom (i.e., the sea depth is constant, also called Pekeris problem). For such a waveguide analytical expressions for the modal amplitudes are well-known, and the modal expansion (1) has the form

$$p(x,y,z) = \frac{\mathrm{i}}{4} \sum_{j=1}^{\infty} \varphi_j(z_s)\, \varphi_j(z)\, H_0^{(1)}\big(k_j \sqrt{x^2+y^2}\big)\,, \tag{45}$$

where $H_0^{(1)}$ denotes the zeroth-order Hankel function of the first kind.

In our example the point source with frequency $f = 25$ Hz is located at $x = y = 0$, $z_s = 100\,\mathrm{m}$ in a 200 m deep shallow sea. The acoustic field is computed at the receiver depth of $z_r = 30\,\mathrm{m}$.

The sound speed $c_w$ and density $\rho_w$ in the sea water and the respective parameters $c_b$ and $\rho_b$ in the bottom have the following values

$$c_w = 1500\ \mathrm{m/s}\,, \quad \rho_w = 1\ \mathrm{g/cm}^3\,, \quad c_b = 1700\ \mathrm{m/s}\,, \quad \rho_b = 1.5\ \mathrm{g/cm}^3\,.$$

For the given frequency and the given set of the parameters the waveguide supports 3 trapped (waterborne) modes, that are taken into account when computing acoustical field in this section (continuous spectrum modes are neglected).

The modal wavenumbers $k_j$ and their respective eigenfunctions $\varphi_j(z)$ were precomputed by the CAMBALA code [53] based on the finite-difference discretization of acoustical spectral problem. Note that the results presented below were obtained by the SSP method and PMLs for the artificial domain truncation (although in all considered examples the codes based on the WAMPE solution technique and the use of discrete TBCs instead of the PML produce absolutely identical results).

A better understanding of the performance of considered starters can be provided by a direct comparison of the resulting solution at some range from the source $r = \sqrt{x^2+y^2} = r_0 = \mathrm{const}$. Such comparison is presented in Fig. 2 for $r = r_0 = 3$ km. Sound pressure level at this range is can be considered as a function of the polar angle $\alpha$ on the interval $[-\pi/2, \pi/2]$. Due to the problem

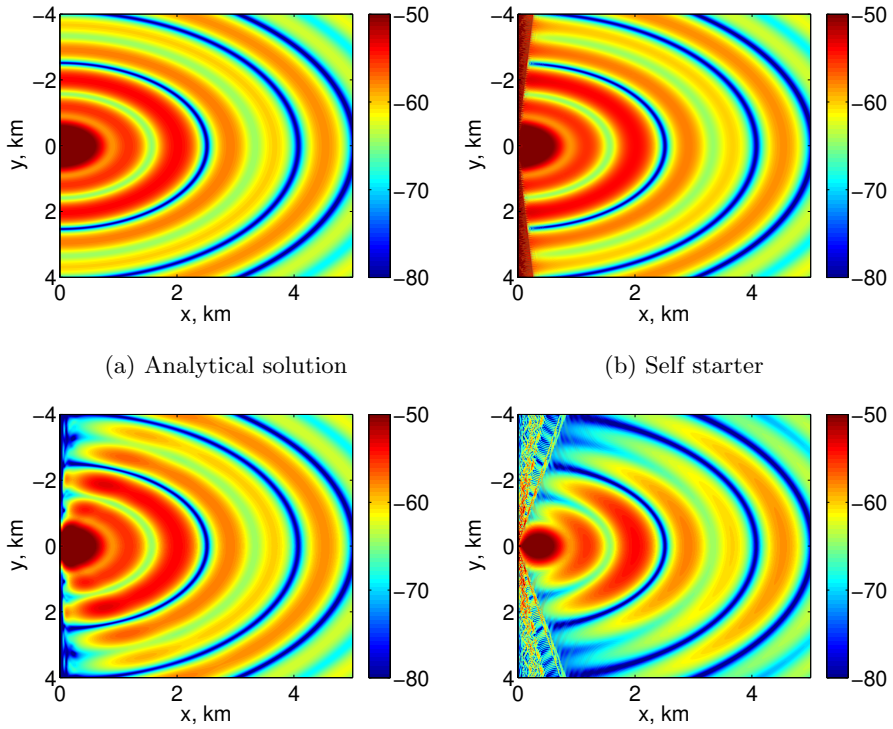


(a) Analytical solution

(b) Self starter

(c) Ray-based starter

(d) Greene starter

Figure 1: Contour plots of acoustical field magnitude $|P(x, y, z = z_r)|$ (in dB re 1 m from the source).

symmetry, the analytical solution at $r = r_0$ is constant, while the WAMPE solutions exhibit some inaccuracies for sufficiently large values of $\alpha$. Firstly, one can see that at this relatively small range the Greene's starter does not properly excite the waves with grazing angles $|\alpha| > 30°$ (the inaccuracy is more than 1 dB). The wide-angle capabilities of the ray-based starter are clearly much better, and the resulting solution is very smooth. The propagation angles $\alpha$ up to 75° can be handled by this starter with the error of no more than 1dB. Theoretically, the self-starter ensures this accuracy for even larger aperture $|\alpha| < 80°$. However, this can be achieved only by using very small step in range $h \leq 2$ m due to the presence of spurious oscillations clearly visible in Fig. 2. For larger steps the solution becomes unstable and can unexpectedly blow up for a

certain mode thus totally spoiling the computed acoustical field. By contrast, the computations with the ray-based IC are much more robust, and the accuracy of 1dB within the interval $|\alpha| < 75^\circ$ is maintained up to $h = 250$ m. From this

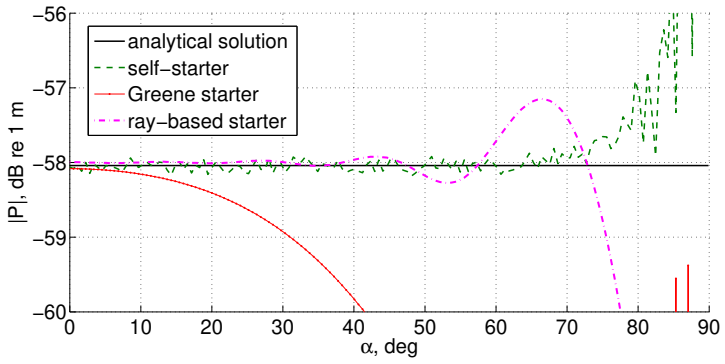


Figure 2: Sound pressure (1 dB re 1 m) as a function of polar angle $\alpha$ at $r = r_0 = 3$ km computed using various starters.

example we conclude that the ray-based starter is apparently the best option for the solution of WAMPEs, and hence it is used in all remaining examples in this study.

Note that if the acoustical field is computed in a stripe of a fixed width of few kilometres then the results at long range from the source will be identical for all starters. However, spurious oscillations triggered by the starter can also propagate long distances and eventually spoil the solution at some unexpected point.

### *7.2. The penetrable wedge: 3D ASA benchmark problem*

In the second example we consider sound propagation in a coastal wedge formed by the sea surface and the sloping penetrable bottom (see Fig. 3). This is a standard test problem which is used for the validation of 3D sound propagation models in underwater acoustics. All environment and source parameters are identical to those from the previous example with the exception for bottom relief that is described by the formula

$$h(y) = h_0 + \tan(\gamma) y \,,$$

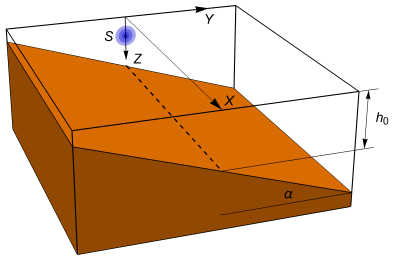


Figure 3: Wedge-like shallow-water waveguide. The $y$ axis is aligned along the bottom slope.

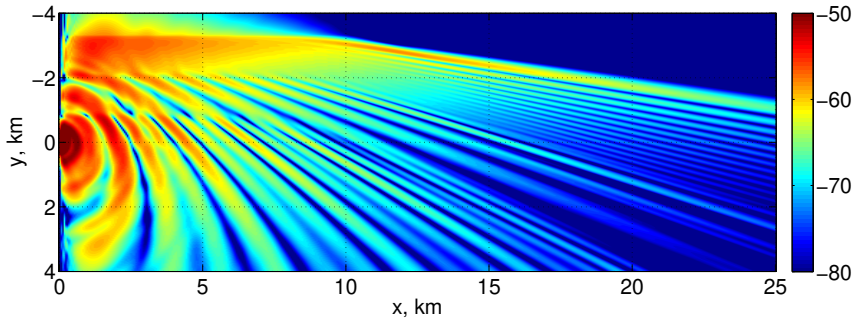


Figure 4: Contour plot of acoustical field (in dB re 1 m) produced by a point source in the coastal wedge (at the depth $z = z_r = 30$ m).

where $h_0 = 200$ m is the water depth at the source location, and $\gamma$ is the bottom slope angle. In this example we set $\gamma = 2.86°$, so that at $y = -4$ km the depth $h(y) = 0$ (i.e., $y = -4$ km represents the coastline). It is known that strong horizontal refraction effects can be observed in this environment, especially for acoustical tracks aligned along the $x$ axis. If the receiver is located at the same isobath as the source, then for each vertical mode there exist two horizontal rays connecting the former and the latter (these rays have the form of hyperbolae). In [7] it was shown that narrow-angle MPE is not capable to properly take the horizontal refraction effects in this problem into account. Thus, involved propagation angles can be covered only by the aperture of a WAMPE. Note that in this problem 3 waterborne modes are excited by the source, and their cut-off depths are reached one by one by acoustical waves propagating upslope. It is widely accepted in acoustical community that this problem cannot be handled

by any adiabatic propagation model.

Our goal is to compute acoustical field at the depth $z_r = 30$ m, and the standard way of benchmarking of various propagation models is to compare the results along $x$ axis (i.e., at $y = 0$). There are several ways to produce a reference solution for this problem, and in this study we use the so-called source images method [54].

The contour plot of acoustical field $P(x, y, z_r)$ (in dB re 1 m) obtained using the WAMPE by the SSP method is shown in Fig. 4. Its comparison with a source images solution is presented in Fig. 5 (as a function of $y$ at $x = 10$ km and $x = 25$ km) and Fig. 6 (as a function of $x$ at $y = 0$). The solid curve in Fig. 6 corresponds to the WAMPE solution for the step $h = 20$ m, but it can be also accurately computed with the range steps up to 1000 m (the markers in Fig. 6 represent the solution obtained with $h = 500$ m. Such step sizes show that SSP technique is extremely computationally efficient, and the theoretical limitations on the step size are posed not by the numerical method but rather by the media variations (typically media parameters, e.g., the depth have significant variation over the horizontal steps of this order).

Note that although our model does not take mode interaction into account, the comparison in Fig. 6 and Fig. 5 highlight excellent agreement of WAMPE computation results with those obtained by the source images methods (that fully takes mode interaction into account). This somewhat unexpected result confirms that in the wedge problem horizontal refraction plays much more important role than the mode coupling effects.

### *7.3. Shallow Sea with Underwater Canyon*

In the third example we consider sound propagation in a shallow sea with an underwater canyon (see schematic in Fig. 7). The bottom relief is described by the formula

$$z = h(y) = h_0 + \Delta h \, \mathrm{sech}^2(\sigma y)\,, \tag{46}$$

where we set $h_0 = 20$ m, $\Delta h = 15$ m, $\sigma = 7 \cdot 10^{-4}$ m$^{-1}$ (i.e., the depth of the canyon is 15 m, and its halfwidth is about 2.5 km).

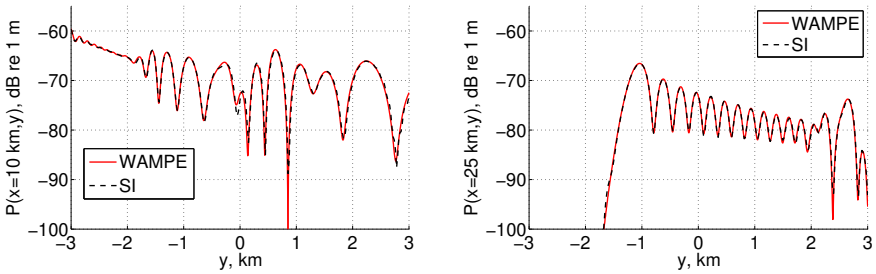


(a) $x = 10$ km (b) $x = 25$ km

Figure 5: Acoustical field in the ASA wedge at $z = z_r = 30$ m as a function of $y$ at $x = 10$ km (a) and $x = 25$ km (b).

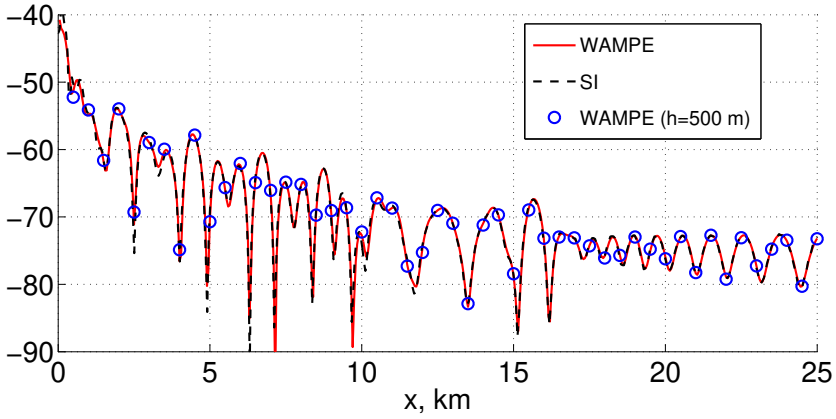


Figure 6: Acoustical field (in dB re 1 m) in the wedge as a function of $x$ for $y = 0$, $z = z_r = 30$ m.

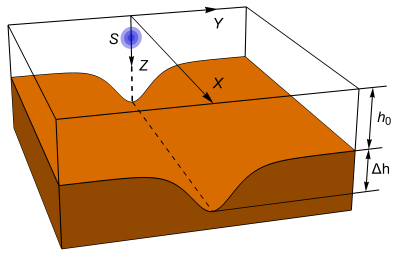


Figure 7: Schematic illustration of an underwater canyon.

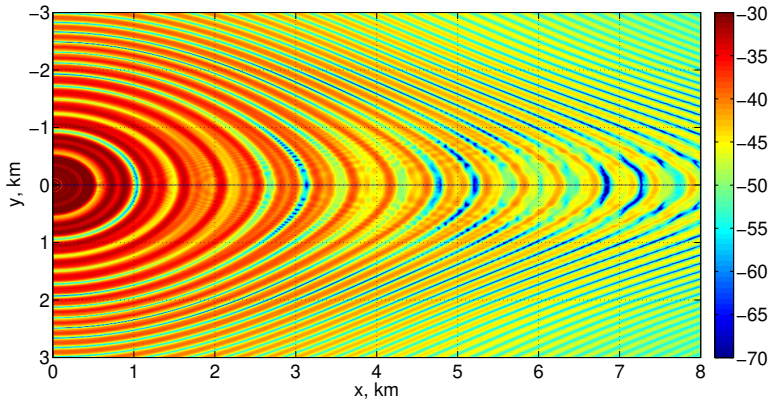


(a) Virtual sources method

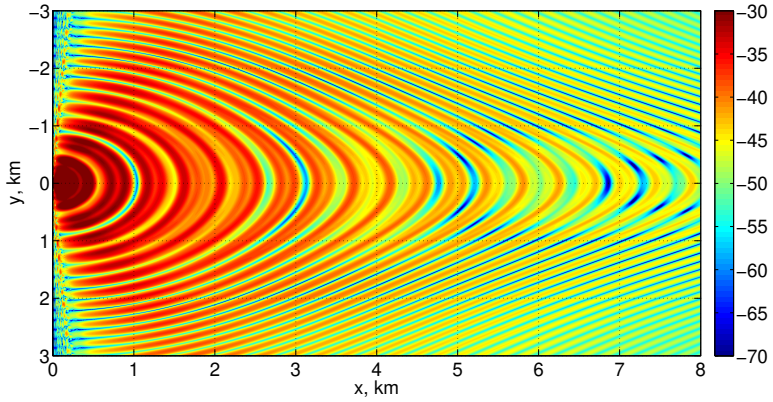


(b) WAMPE SSP solution

Figure 8: Acoustical field (in dB re 1 m from the source) in the shallow sea with underwater canyon at $z = z_s = 10$ m as a function of $x, y$. The field is computed by the virtual sources technique (a) and by solving WAMPE (b).

In this scenario horizontal refraction manifests in the focusing of acoustical energy in the water column over the canyon. The field in the canyon area can be represented in the form of a decomposition over specific horizontal modes studied in [3].

Let us assume that the source of the frequency $f = 150$ Hz is located at the depth $z_s = 10$ m over the canyon axis (i.e., at $y = 0$). For these values of

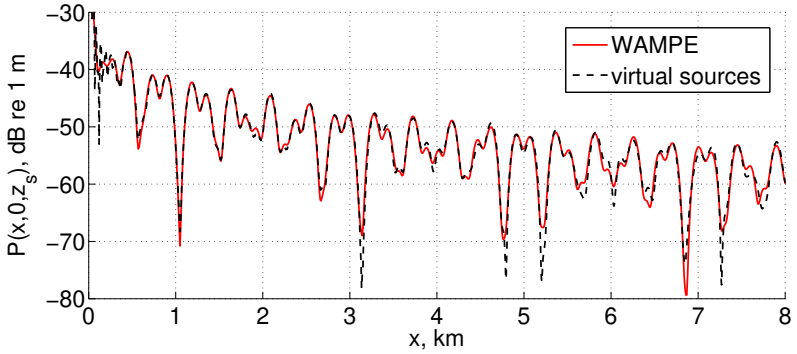


Figure 9: Acoustical field (in dB re 1 m) a shallow sea with underwater canyon as a function of $x$ for $y = 0$, $z = z_r = 30$ m (i.e., along the canyon axis, where the focusing takes place).

the parameters the waveguide supports 4 trapped (waterborne) modes near the channel axis $y = 0$ and only two trapped modes outside the canyon (for large $y$). Thus we can expect strong mode coupling effects associated with upslope propagation of acoustical waves from the canyon axis towards its periphery. On the other hand we should expect focusing of acoustical energy over the canyon caused by the horizontal refraction.

Acoustical field $P(x, y, z_s)$ (in dB re 1 m) as a function of the horizontal coordinates $x, y$ is shown in Fig. 8(b). The reference solution for this case is obtained by the virtual sources approach [55] (see Fig. 8(a)). Just as in the previous example, despite strong mode coupling the fields computed by the two methods look almost identical.

A more detailed comparison is presented in Fig. 9 where acoustical pressure along the channel axis $y = 0$ is plotted as a function of longitudinal coordinate $x$. In this figure small discrepancies caused by the absence of mode coupling in the MPE simulation are noticeable, although the accuracy of the latter is still sufficient for most practical applications of underwater acoustics.

## 8. Conclusion

In this study we systematically develop numerical techniques for the modelling of adiabatic sound propagation. Our approach is based on mode parabolic equations that are capable of simulating horizontal wide-angle refraction effects. These equations are obtained by the Padé approximation of the PDMPE (5) or its propagator (11) (in the SSP approach).

Although the idea to use Padé approximations for the approximation of pseudo-differential operators is by no means new, it has not been systematically discussed in the context of MPEs in the literature until now. Our study shows that adiabatic WAMPEs allow accurate modelling of acoustical field even in the cases when strong (or resonant [7]) mode coupling is expected. At the same time, it is very important that MPEs described in this work have large aperture in the horizontal plane. This feature is crucial, e.g., for the wedge problem (see §7.2). Now the standard reference solution of the ASA wedge problem by the source images method can be replaced by a much more efficient WAMPE solution [16, 15] implemented both in MATLAB and C++.

We also provide a comprehensive treatment of various issues related to the numerical solution of WAMPEs, especially the problems of artificial domain truncation and the proper design of a starter. In particular, it is shown that in most cases the ray-based initial condition proposed here is the most robust and efficient way to simulate the field produced by a point source in the WAMPE framework.

The inability to take mode interaction effects into account still remains the main shortcoming of adiabatic MPEs, and our main challenge for the future work is to overcome it. However, as can be seen from the examples presented here, even adiabatic MPEs can produce highly accurate solutions for the problems where the mode interaction seems to play an important role (see §7.2 and §7.3). It is also obvious that MPEs are in general the fastest and most robust approach for the simulation of acoustical fields in 3D ocean environments.

**Acknowledgements**

The major part of this study was accomplished during the visit of P.P. to the University of Wuppertal partly supported by the Heinrich Hertz Foundation. The work was also supported by the Russian Foundation for Basic Research under the contracts No. 18-05-00057_a and No. 18-35-20081_mol_a_ved. A.T. and P.P. were also partly supported by the POI FEBRAS Program "Mathematical simulation and analysis of dynamical processes in the ocean" (No. 0271-2019-0001).

**References**

[1] F. B. Jensen, W. A. Kuperman, M. B. Porter, H. Schmidt, Computational ocean acoustics, Springer Science & Business Media, 2011.

[2] R. Burridge, H. Weinberg, Horizontal rays and vertical modes, in: Wave propagation and underwater acoustics, Springer, 1977, pp. 86–152.

[3] P. S. Petrov, T. N. Petrova, Asymptotic solution for the problem of sound propagation in a sea with an underwater canyon, J. Acoust. Soc. Amer. 136 (4) (2014) EL281–EL287.

[4] M. D. Collins, The adiabatic mode parabolic equation, J. Acoust. Soc. Amer. 94 (4) (1993) 2269–2278.

[5] M. Y. Trofimov, Narrow-angle parabolic equations of adiabatic single-mode propagation in a horizontally inhomogeneous shallow sea, Acoust. Phys. 45 (1999) 575–580.

[6] A. Abawi, W. Kuperman, M. Collins, The coupled mode parabolic equation, J. Acoust. Soc. Amer. 102 (1) (1997) 233–238.

[7] M. Y. Trofimov, S. Kozitskiy, A. Zakharenko, A mode parabolic equation method in the case of the resonant mode interaction, Wave Motion 58 (2015) 42–52.

[8] P. S. Petrov, F. Sturm, An explicit analytical solution for sound propagation in a three-dimensional penetrable wedge with small apex angle, J. Acoust. Soc. Amer. 139 (3) (2016) 1343–1352.

[9] P. S. Petrov, S. V. Prants, T. N. Petrova, Analytical Lie-algebraic solution of a 3D sound propagation problem in the ocean, Physics Letters A 381 (2017) 1921–1925.

[10] P. N. Petrov, P. S. Petrov, Asymptotic solution for the problem of sound propagation in a shallow sea with the bathymetry described by a parametric quadratic function, J. Acoust. Soc. Amer. 146 (3) (2019) 1946–1955.

[11] M. Y. Trofimov, A. D. Zakharenko, S. B. Kozitskiy, Mode Gaussian beam tracing, Comput. Phys. Commun. 207 (2016) 179–185.

[12] A. C. Antoulas, Approximation of large-scale dynamical systems, Vol. 6, SIAM, 2005.

[13] M. S. Ballard, J. D. Sagers, Measurements and modeling of acoustic propagation in a scale model canyon, J. Acoust. Soc. Amer. 146 (3) (2019) 1858–1866.

[14] A. Rutenko, S. Kozitskii, D. Manulchev, Effect of a sloping bottom on sound propagation, Acoustical Physics 61 (1) (2015) 72–84.

[15] Acoustic: Wide-angle mode parabolic equation (WAMPE) solver for Helmholtz equation, `https://github.com/GoldFeniks/Acoustic`, accessed: 2019-11-23.

[16] MPE: Mode parabolic equations, their solutions and test cases, `https://github.com/kaustikos/MPE`, accessed: 2019-11-23.

[17] L. Fishman, A. Gautesen, Z. Sun, Uniform high-frequency approximations of the square-root Helmholtz operator symbol, Wave Motion 26 (1997) 127–161.

[18] L. Fishman, One-way wave equation modeling in two-way wave propagation problems, in: B. Nilsson, L. Fishman (Eds.), Mathematical Modelling of Wave Phenomena 2002, Mathematical Modelling in Physics, Engineering and Cognitive Sciences 7, Växjö University Press, Växjö, Sweden, 2004, pp. 91–111.

[19] J. F. Claerbout, Fundamentals of geophysical data processing with application to petroleum prospect, McGraw-Hill, 1976.

[20] M. D. Collins, A split-step Padé solution for the parabolic equation method, J. Acoust. Soc. Amer. 93 (1993) 1736–1742.

[21] V. Avilov, Pseudodifferential parabolic equations of sound propagation in the slowly range-dependent ocean and its numerical solution, Acoustical Physics 41 (1995) 1–7.

[22] M. Lytaev, Nonlocal boundary conditions for split-step Padé approximations of the Helmholtz equation with modified refractive index, IEEE Antenn. Wireless Propag. Lett. 17 (8) (2018) 1561–1565.

[23] M. E. Taylor, Pseudo Differential Operators, Springer, 1974.

[24] F. Milinazzo, C. Zala, G. Brooke, Rational square-root approximations for parabolic equation algorithms, J. Acoust. Soc. Amer. 101 (1997) 760–766.

[25] X. Antoine, Y. Huang, Y. Y. Lu, Computing high-frequency scattered fields by beam propagation methods: A prospective study, J. Algor. & Comput. Techn. 4 (2) (2010) 147–166.

[26] M. Ehrhardt, A. Zisowsky, Discrete non-local boundary conditions for split-step Padé approximations of the one-way Helmholtz equation, J. Comput. Appl. Math. 200 (2007) 471–490.

[27] S. L. Chui, Y. Y. Lu, A propagator-/spl theta/beam propagation method, IEEE Photon. Techn. Lett. 16 (3) (2004) 822–824.

[28] O. Ozgun, G. Apaydin, M. Kuzuoglu, L. Sevgi, Petool: Matlab-based one-way and two-way split-step parabolic equation tool for radiowave propagation over variable terrain, Comput. Phys. Commun. 182 (12) (2011) 2638–2654.
URL http://cpc.cs.qub.ac.uk/summaries/AEJS_v1_0.html

[29] A. Arnold, M. Ehrhardt, A transparent boundary condition for an elastic bottom in underwater acoustics, in: I. Dimov, I. Farago, L. Vulkov (Eds.), Finite Difference Methods,Theory and Applications. FDM 2014, Lecture Notes in Computer Science, Vol. 9045., Springer, Cham, 2015, pp. 15–24.

[30] J.-P. Bérenger, A perfectly matched layer for the absorption of electromagnetic waves, J. Comput. Phys. 114 (1994) 185–200.

[31] W. Chew, W. Weedon, A 3-D perfectly matched medium from modified Maxwell's equations with stretched coordinates, Micro. Opt. Lett. 7 (1994) 599–604.

[32] M. Levy, Perfectly matched layer truncation for parabolic wave equation models, Proc. Roy. Soc. Lond. A 457 (2001) 2609–2624.

[33] Y. Lu, J. Zhu, Perfectly matched layer for acoustic waveguide modeling – benchmark calculations and perturbation analysis, CMES. Computer Modeling in Engineering & Sciences 22.

[34] T. Hagstrom, New results on absorbing layers and radiation boundary conditions, in: Topics in computational wave propagation, Vol. 31 of Lect. Notes Comput. Sci. Eng., Springer, Berlin, 2003, pp. 1–42.

[35] X. Antoine, A. Arnold, C. Besse, M. Ehrhardt, A. Schädle, A review of transparent and artificial boundary condition techniques for linear and nonlinear Schrödinger equations, Commun. Comp. Phys. 4 (2008) 729–796.

[36] V. A. Baskakov, A. V. Popov, Implementation of transparent boundaries for numerical solution of the Schrödinger equation, Wave Motion 14 (1991) 123–128.

[37] J. Papadakis, Exact nonreflecting boundary conditions for parabolic-type approximations in underwater acoustics, J. Comput. Acous. 2 (1994) 83–98.

[38] A. V. Popov, Accurate modeling of transparent boundaries in quasi-optics, Radio Science 31 (6) (1996) 1781–1790.

[39] M. Ehrhardt, Discrete artificial boundary conditions, Ph.D. thesis, Technische Universität Berlin, Berlin (2001).

[40] B. Mayfield, Non-local boundary conditions for the Schrödinger equation, Ph.D. thesis, University of Rhode Island, Providence, RI (1989).

[41] P. Petrov, M. Ehrhardt, On Mayfield's stability proof for the discretized transparent boundary condition for the parabolic equation, Appl. Math. Lett. 44 (2015) 45–49.

[42] G. Brooke, D. Thomson, Non-local boundary conditions for high-order parabolic equation algorithms, Wave Motion 31 (2000) 117–129.

[43] T. Friese, F. Schmidt, D. Yevick, Transparent boundary conditions for a wide-angle approximation of the one-way Helmholtz equation, J. Comput. Phys. 165 (2000) 645–659.

[44] F. Schmidt, T. Friese, D. Yevick, Transparent boundary conditions for split-step Padé approximations of the one-way Helmholtz equation, J. Comput. Phys. 170 (2001) 696–719.

[45] A. Arnold, M. Ehrhardt, Discrete transparent boundary conditions for wide angle parabolic equations in underwater acoustics, J. Comput. Phys. 145 (1998) 611–638.

[46] D. Mikhin, Exact discrete nonlocal boundary conditions for high-order Padé parabolic equations, J. Acoust. Soc. Amer. 116 (2004) 2864–2875.

[47] D. Mikhin, Analytic discrete transparent boundary conditions for high-order Padé parabolic equations, Wave Motion 45 (2008) 881–894.

[48] M. Ehrhardt, Discrete transparent boundary conditions for Schrödinger-type equations for non-compactly supported initial data, Appl. Numer. Math. 58 (2008) 660–673.

[49] M. Ehrhardt, A. Arnold, Discrete transparent boundary conditions for the Schrödinger equation, Riv. Mat. Univ. Parma 6 (2001) 57–108.

[50] A. Zisowsky, Discrete transparent boundary conditions for systems of evolution equations, Ph.D. thesis, Technische Universität Berlin, Berlin (2003).

[51] R. R. Greene, The rational approximation to the acoustic wave equation with bottom interaction, J. Acoust. Soc. Amer. 76 (1984) 1764–1773.

[52] M. D. Collins, A self-starter for the parabolic equation method, J. Acoust. Soc. Amer. 92 (4) (1992) 2069–2074.

[53] CAMBALA: Coupled Acoustic Modes, `https://github.com/Nauchnik/Acoustics-at-home`, accessed: 2019-11-23.

[54] J. Tang, P. Petrov, S. Piao, S. Kozitskiy, On the method of source images for the wedge problem solution in ocean acoustics: Some corrections and appendices, Acoustical Physics 64 (2) (2018) 225–236.

[55] A. T. Abawi, M. B. Porter, Propagation in an elastic wedge using the virtual source technique, J. Acoust. Soc. Amer. 121 (3) (2007) 1374–1382.